Soft matter, Volume XX

Supporting Material

Carbon nanotube transmembrane channel formation and single-stranded DNA spontaneous internalization. A Dissipative Particle Dynamics study.

A. Valdivia[a] and C. Jaime[a]

[a] Department de Química, Universitat Autònoma de Barcelona, 08193 Bellaterra (Cerdanyola del Vallès), Barcelona, Spain

All the simulations are performed using a Fortran90 software originally coded by prof. Smit's group (M. Kranenburg,[1,2] M. Venturoli,[3] F. de Meyer,[4,5] J. M. Rodgers,[6] A. Benjamini[7] and modified, in part, by ourselves).

Dissipative Particle Dynamics.

As time evolves, the velocities and new trajectories must be determined by Newton's laws. Among the different existing methods, in this case, a modified version of the velocity-Verlett algorithm[8] is used following Groot and Warren (1997).[9] In their paper, they explained that temperature can be controlled by three factors, the time step Δt, the noise level σ, and the λ in the Verlet algorithm. We used a density of $\rho = 3$, $\sigma = 3$, $\lambda = 0.65$ and $\Delta t = 0.03$ or $\Delta t = 0.06$ (indicated when necessary).

DPD-Monte Carlo (DPD-MC): tensionless bilayer

As mentioned in the introduction, the DMPC bilayer is simulated in the tensionless state following Venturoli and Smit (1997).[3] In summary, they adopted a hybrid scheme in which DPD is used to evolve the positions of the particles and the Monte Carlo method for imposing a given value of surface tension, $\gamma = 0$ in this case. As explained in the mentioned paper, this is done by changing the bilayer projected area on the plane perpendicular to the bilayer normal, A, by an amount ΔA at the same time that the high of the simulation box is changed to maintain the total volume constant, ensuring that no work is done against external pressure and leading to a formal (N, γ, T) ensemble.

The described hybrid approach is only used for the pure DMPC bilayer simulations, the rest of the simulations using the equilibrated bilayers, are done in the conventional DPD approach, i.e. in the (N, V, T) ensemble. For more details, see the cited paper from Venturoli and Smit.

The soft repulsion parameter (a_{ij}) for water

Following Groot and Warren (1997)[9], the soft repulsion parameter (a_{ij}) for the water-water interaction is set in such a way that matches the experimental dimensionless compressibility of water at room temperature ($k^{-1} = 15.9835 \approx 16$ at $300K$). They found that the compressibility of water is matched for a bead density $\rho > 2$ under the following relation

$$k^{-1} = 1 + 2\alpha a_{WW}\rho / k_B T \tag{1}$$

where $\alpha = 0.101 \pm 0.001$. Then, and since a density ρ of 3 has been chosen, a soft repulsion parameter of $a_{WW} = 25$ should be used according to **eq. 1**. Notice that this value, should be used when a single water molecule is being represented by one DPD particle. In this work, we represent three water molecules in a single DPD particle using the same soft repulsion parameter instead of the value of $a_{WW} = 78$ that should be employed. Below, an explanation on why this approach is used, is provided after some details on how the time and length scales are fitted.

Reduced units, time- and length-scales

As common in DPD, we use reduced units defining $k_B T_0 = 1$ where T_0 is room temperature, and r_C as the unit of length. Bead masses, *m*, are considered to be 1.0. Following Groot and Warren (1997)[9], the length scale depends on the bead density ρ and the number of (water) molecules represented by one bead N_m or "mapping factor". The bead density ρ is the number of DPD particles N_w divided by the volume V (in units of r_C^3): $\rho = N_w/V$. Taking the experimental volume of one H_2O molecule as $30\ \text{Å}^3$ from Lu et al. (1993),[10] a DPD bead with a mapping factor of $N_m = 3$ represents a volume of $90\ \text{Å}^3$. Since the bead density is $\rho r_C^3 = 3$, a cube of r_C^3 volume contains 3 beads corresponding to a volume of $270\ \text{Å}^3$, leading to a physical interaction radius of

$$r_C = \sqrt[3]{270} = 6.4633\ \text{Å} \tag{2}$$

For the time scale, we follow Groot and Rabone (2001)[11] and the self-diffusion constant of water beads is matched with the experimental self-diffusion constant of water at room temperature calculated by Partington et al. (1952)[12] to be $D_{water} = (2.43 \pm 0.01)\ x\ 10^{-5} cm^2/s$.

From Groot (2003),[13] the following general relation is found relating the simulated self-diffusion constant of water beads when $a_{WW} = 25$ with the experimental value:

$$\tau = \frac{N_m D_{sim} r_C^2}{D_{water}} = 25.7 \pm 0.1 N_m^{5/3}. \tag{3}$$

This implies that for a mapping factor of $N_m = 3$, $a_{WW} = 25$ and a bead density $\rho = 3$, the time unit corresponds to $160.4\ ps$ and time steps of $\delta t = 0.03\tau$ and $\delta t = 0.06\tau$ are used, corresponding to $\sim 4.8\ ps$ and $\sim 9.6\ ps$, respectively.

As explained above, following **eq. 1** a soft repulsion parameter of $a_{WW} = 78$ should be used in this case, since a mapping factor of $N_m = 3$ is employed, to match the same water compressibility obtained for one water molecule per bead ($k^{-1} \approx 16$). However, the work of Kranenburg *et al.*[2] for the DMPC bilayer demonstrate that the soft repulsion parameters derived for a mapping factor of $N_m = 1$ and $N_m = 3$ were, in the case of lipid bilayer DPD simulations, interchangeable since the a_{ij} scale is a relative scale. As can be seen from **eq. 3**, R. Groot also notice that fact.

DPD-quantum mechanics combination

The energies obtained for all the components discussed in this article as well the assigned soft repulsion parameters a_{ij}, can be found below in **Tables 1**, **2** and **3**.

Table 1 Molecular fragments considered for each bead and its symbol for DMPC lipids, the calculated solvation energies for each fragment following and the a_{iW} value assigned.

Molecular fragment	Symbol	$E_{i,\ solvent}$ $(kcal/mol)$	$E_{i,\ gas-phase}$ $(kcal/mol)$	$E_{i,\ solvation}$ $(kcal/mol)$	a_{iW}
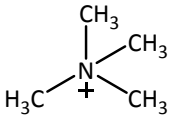	H	− 134460.95	− 134409.78	− 51.17	−
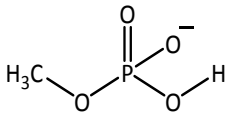	H	− 428620.21	− 428556.41	− 63.80	−
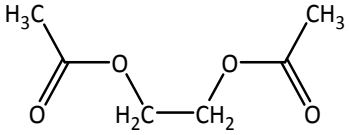	H	− 336122.86	− 336116.18	− 6.68	−
Average between head groups	H	− 299734.67	− 299694.12	− 40.55	15
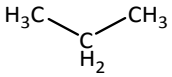	t	− 74776.29	− 74776.16	− 0.13	80

Table 2 Molecular fragments considered for SWCNT beads and its symbol, the calculated solvation energy and the a_{iW} value assigned.

Molecular fragment	Bead symbol	$E_{i,\ solvent}$ $(kcal/mol)$	$E_{i,\ gas-phase}$ $(kcal/mol)$	$E_{i,\ solvation}$ $(kcal/mol)$	a_{iW}
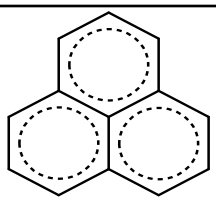	CNT	− 314295.52	− 314292.69	− 2.83	75

Table 3 Molecular fragments considered for ssDNA beads and its symbol, the calculated solvation energy and the a_{iW} value assigned.

Molecular fragment	Bead symbol	$E_{i,\ solvent}$ $(kcal/mol)$	$E_{i,\ gas-phase}$ $(kcal/mol)$	$E_{i,\ solvation}$ $(kcal/mol)$	a_{iW}
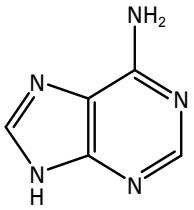	A	− 293283.29	− 293273.93	− 9.35	65
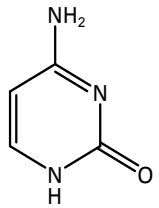	C	− 247862.73	− 247847.51	− 15.22	55
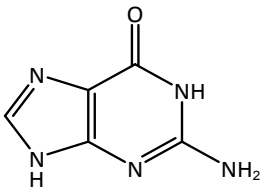	G	− 340504.89	− 340487.60	− 17.29	52
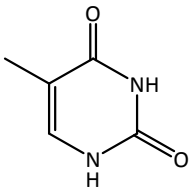	T	− 285013.22	− 285002.41	− 10.82	62

Coarse-grained Models and parameters

Pure DMPC bilayer

Table 4 Soft repulsion parameters a_{ij} used in this article for a pure DMPC lipid bilayer proposed by Kranenburg et al. (2004).[2]

a_{ij}	**W**	**t**	**H**
W	25	80	15
t		25	80
H			35

Additional space in the simulation box is needed for the CNT transmembrane channel simulations, more water beads are needed for maintaining the density at $\rho = 3$. Therefore, instead using 25 water beads per lipid to ensure the fully hydrated bilayer, as in the case of the mentioned papers, we use 60 water beads per lipid. The reason for the unexpected phase is attributed to this fact and is further discussed below.

To characterize the behaviour of the simulated bilayers, the data about the lipid tail tilt angle, θ_{tilt}, the order parameter S_{tail}, the hydrophobic thickness, d_L^o , and the bilayer normal area, A, is collected every 5 cycles and averaged, i.e. over 12000 independent configurations.

The order parameter is defined as

$$S_{tail} = \frac{1}{2}\left\langle 3\ cos^2\theta_{tilt} - 1 \right\rangle \tag{4}$$

where θ_{tilt} is the angle between the vector defined by the first and the last bead of each lipid and the bilayer normal. The order parameter has a value of 1 if the vector is, on average, parallel to the bilayer normal, a value of 0 if the orientation is random and a value of -0.5 if the vector is, on average, perpendicular to the bilayer normal, i.e. parallel to the bilayer plane. Hence, a phase transition is determined by the inflection point in the order parameter as temperature is increasing. For the bilayer hydrophobic thickness, the value is estimated by calculating the difference between the average positions along the bilayer normal (i.e. the x direction) of the first tail bead attached to the first head group of all the lipids in one monolayer (*top*), and the lipids in the opposite monolayer (*bottom*),

$$d_L^o = \left\langle \bar{x}_t^{top} - \bar{x}_t^{bottom} \right\rangle, \tag{5}$$

where x_t is the x position of the first tail bead of each lipid plus the bead radius (considering that each DMPC has 2 tails).[14] For obtaining the area per lipid, A_L, the computed average bilayer normal area is taken and divided by the amount of lipids in one monolayer, i.e. 450 lipids in this case.

Therefore, pure DMPC bilayers are simulated over 80000 DPD-MC cycles with a time step of $\delta t = 0.06\tau$, from which 20000 are done to equilibrate the system without collecting data. In each cycle is chosen, with a probability of 70%, whether to perform a random number between 1 and 50 DPD steps, or to attempt to change the simulation box aspect ratio according to the imposed value of surface tension $\gamma = 0$. The quantities of interest are collected every 5 cycles, and averaged, i.e. over 12000 independent configurations.

The pre-transition is observed at $T_{pre}^* = 0.325$. Below this temperature, the computed tail order parameter, S_{tail}, grows slowly reaching 0.77 at $T^* = 0.250$ (8.3 ℃), where the sub-transition is observed. This high value on S_{tail} at low temperatures is an indicative of lipid tail order. The S_{tail} does not reach the value of 1 (ordering parallel to the bilayer normal) at this low temperature due to an average tilt angle with respect the bilayer normal of about $\theta_{tilt} = 23°$. As explained by Koynova and Caffrey (1998)[15], depending on the structural composition of the lipid head groups, the gel phase is L_β phase (for example in phosphatidylethanolamines) where the tails are ordered and parallel to the

bilayer normal, or $L_{\beta'}$ (for example in phosphatidylcholines, as in this case) where the tails show a tilt angle with respect to the bilayer normal.

Above $T^*_{pre} = 0.325$ the system changes from $L_{\beta'}$ phase to the $P_{\beta'}$ or rippled gel phase.[14, 15] When $0.425 > T^* > 0.325$ the system is in the $P_{\beta'}$ or rippled phase and the bilayer shows some regions in the gel-phase $L_{\beta'}$ and others in the fluid phase L_α, indicating that a transition below the melting temperature is taking place. In this window of temperatures, the S_{tail} falls from ~ 0.7 to ~ 0.43 indicating that the order of tails is being lost as the temperature increases. Above the melting temperature, $T^*_m = 0.425$, the system is in the so-called L_α, liquid crystalline or fluid phase, where the lipids are randomly distributed. The S_{tail} slowly decreases while temperature is raised reaching the value of 0.19 at $T^* = 1$, the highest temperature simulated corresponding to ~ 76 ℃, indicating that the lipids tail segments have a very low order due to the overlap between the monolayers.

The quantitative performance of the simulated bilayers is also examined by comparing the computed values for the pure bilayer hydrophobic thickness, d_L^o, and the area per lipid, A_L, with the values derived from experimental reports at different temperatures, shown in **Table 5**, for fully hydrated pure DMPC lipid bilayers. The values obtained from the simulations are in good quantitative agreement with the experimental values and only for $T = 10$ ℃ the computed bilayer hydrophobic thickness and the area per lipid deviate a bit more, even if the experimental errors are considered.

Table 5 Values obtained from the simulations in this study and from various experimental studies for the pure DMPC bilayer hydrophobic thickness, d_L^o, and the area per lipid, A_L.

	d_L^o(Å)		A_L(Å^2)	
T (°C)	Simulation	Experiment	Simulation	Experiment
10	34.5	30.3*	44.0	47.2*
30	26.3	25.6†	59.1	60.0†
		25.7‡		59.9‡
		26.2§		59.6§
50	23.9	24.8‡	63.8	63.3‡
		24.0†		65.4†
60	23.1	24.1‡	65.5	65.7‡
65	22.8	23.4†	66.3	68.5†

* From Tristram-Nagle et al. (2002).[16]

† From Petrache et al. (2000).[17]

‡ From Kučerka et al. (2011).[18]

§ From Tristram-Nagle et al. (2000).[19]

Single-walled carbon nanotubes (SWCNTs)

The model is built as follows:

- CNT wall beads have a cut-off diameter equal to the cut-off distance $r_c = 1\ (6.4633\ \text{Å})$.
- Considering the bond lengths between carbon atoms in CNTs as $d_{C=C} = 1.44\ \text{Å}$,[20] a bead of symbol "CNT" consists on a phenalene-type molecular fragment as shown in **Fig. 2 in the main text**. The approximation implies that the molecular fragment of choice fits into the cut-off diameter of simulated beads, $r_c = 1$. Thus, the experimental molar volume of phenalene has not been considered.
- The bond equilibrium length between two consecutive nanotube wall beads is chosen as $r_0 = 0.77\ (\sim 4.99\ \text{Å})$. This value corresponds to the distance between two consecutive phenalene structures, coinciding with the length-in-plane of a single phenalene as shown in **Fig. 2 in the main text**.
- Each circular layer of beads that compose the cylinder, is rotated to achieve an alternated pattern as shown in **Fig. 2 in the main text**. The angle of rotation is $\theta_{rot} = 360°/beads\ per\ layer$, i.e. depends on the nanotube diameter. This is done for avoiding larger hollow spaces between wall beads.
- To maintain the constant cylindrical structure, the beads on each ring are connected to its homologue at a diameter distance by virtual bonds. The harmonic spring constant for all nanotube connected beads is $K_r = 180$ and the bending constant is $K_\theta = 55$. The angle defined by two beads of a layer with a bead of the next layer is $\theta_0 = 53°$ as shown in **Fig. 2 in the main text**.

Single-stranded DNA (ssDNA)

The model is built as follows:

- The chains have 6 different bead types: "A" for adenine, "C" for cytosine, "G" for guanine, "T" for thymine, "PEN" for pentose and "PHOS" for phosphate, each one with a colour assigned as shown in **Fig. 1**. All beads have a cut-off diameter equal to the cut-off distance $r_c = 1\ (6.4633\ \text{Å})$ except the phosphate bead, which diameter is reduced in a $15\ \%$ considering its smaller molecular size, i.e. $r_c = 0.85$.
- The bond lengths and angles values are similar to those used by Knotts et al. (2007)[21] for helical DNA considering the B-isoform.[22] Nevertheless, here a ssDNA chain is modelled and the helical structure is not considered. The bond lengths reported in the mentioned paper are changed as follows:
  - The bonds between phosphates and pentoses are considered equal with an equilibrium length of $r_0 = 0.4904\ (\sim 3.17\ \text{Å})$ with a spring constant of $K_r = 170$. This distance implies a 15% of reduction from the reported value $(3.729\ \text{Å})$,[21] considering that beads are connected from its centres of masses.
  - The bond lengths between the nucleic acid bases and pentoses are reduced a 45% from the reported values,[15] considering that the centre of mass of each nucleic acid base is in the centre of mass of one bead. Its values in reduced units are: $r_0 = 0.5472$ for adenine, $r_0 = 0.4188$ for cytosine, $r_0 = 0.5439$ for guanine and $r_0 = 0.4153$ for thymine.

- The distance between two consecutive nucleic acid bases in the chain is fixed at $0.526\ (34\ \text{Å})$ corresponding to the experimental spacing in B-DNA.[22]
- The angles between phosphates beads and pentose beads are $\theta_0 = 65°$ and between pentose beads and all nucleic acid bases $\theta_0 = 148°$. All the bending constant are $K_\theta = 55$. By this, the approximate dimensions of a real ssDNA chain are represented, known as ~ 10 residues per turn of $\sim 36°$ if the helical B-DNA isoform is considered.[30]

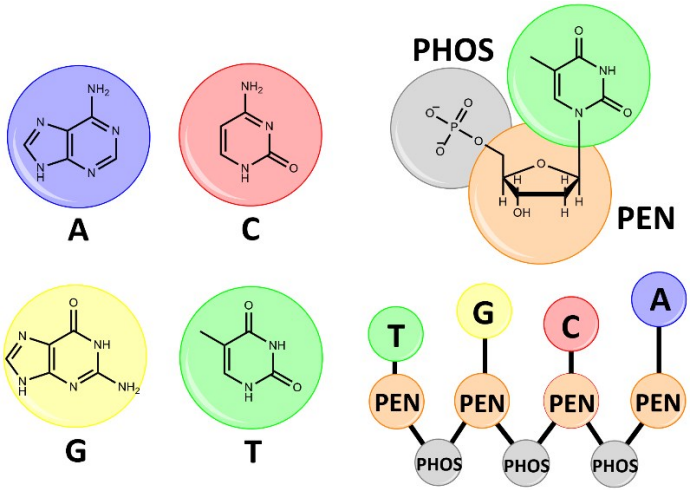

Fig. 1 Scheme of the coarse-grained model for ssDNA used in this article. The letters indicate the symbol of each bead, the colours are set for differentiate each type of bead and are maintained in the simulation snapshots: A blue, C red, G yellow, T lime, PEN orange and PHOS grey.

The hydration energies obtained here by hybrid-DFT calculations, shown in **Table 3** differ from the reported experimental values: $\sim -21\ kcal/mol$ for guanine, $\sim -18\ kcal/mol$ for cytosine, $\sim -12\ kcal/mol$ for adenine and thymine.[23] The deviations are due to the relatively simple level of calculation used in this study. Even though, the values are close to the experimental ones and the tendency between them is kept.

SWCNTs spontaneous piercing process

The simulated bilayer hydrophobic thickness at this temperature is $d_L^o = 26.03\ \text{Å}\ (2.6\ nm)$ and the spontaneous piercing of SWCNTs is examined for both pristine SWCNTs and SWCNTs with polar rims. To obtain the angle θ_{CNT} with respect the bilayer plane (yz in this case), the module of the vector defining the length of the cylindrical SWCNT (L_{CNT}) is calculated from the centre points in the first and the last rings of beads in the SWCNT model. Using this value as the hypotenuse c, of a right triangle and the side a, defined as the difference between the x coordinates of the centre up and bottom points, the angle is calculated as

$$90° \geq \theta_{CNT} = \sin^{-1}\frac{a}{c} \geq 0° \quad . \tag{6}$$

Hence, the tilt angle with respect the bilayer normal is calculated as follows

$$90° \geq \theta_{tilt} = 90° - \theta_{CNT} \geq 0° . \tag{7}$$

The mean SWCNT tilt angle with respect the bilayer normal, once the CNTs are stabilized, is examined as function of the SWCNT length, L_{CNT}, and considering the three different inner diameters employed. The concept of hydrophobic mismatch is used and defined as

$$\Delta_{HM}^{o} = L_{CNT}^{H} - d_{L}^{o}, \tag{8}$$

where L_{CNT}^{H} is the hydrophobic SWCNT length (without the polar rims beads if present) and d_{L}^{o} is the bilayer hydrophobic thickness obtained from each simulation. The point where the SWCNT angle is stabilized is determined by fitting the tilt angle θ_{tilt} change as function of simulated time and finding when the value becomes stable and approximately equal to the mean value. The plot for the tilt angle θ_{tilt} vs L_{CNT} as function of the piercing time is shown in **Fig. 2** below and discussed in the main paper.

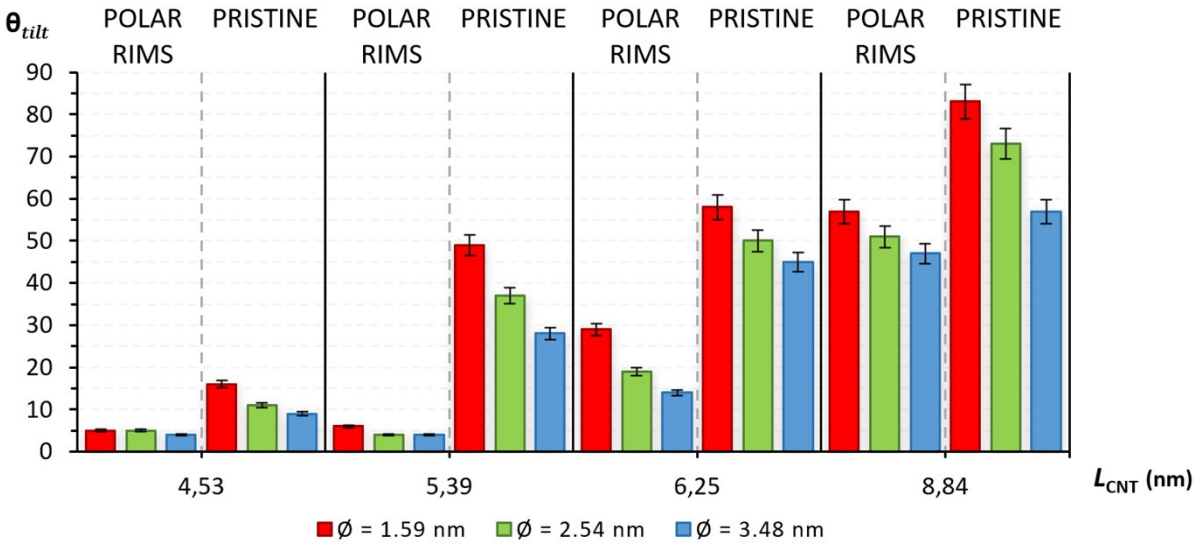

Fig. 2 SWCNT tilt angle θ_{tilt} as function of nanotube total length L_{CNT} and diameter $\emptyset_{CNT}$ for both pristine SWCNTs (P.) and SWCNTs with polar rims (P.R.).

The general tendency on the time dependence of the piercing process is not so straightforward as shown in **Fig. 3**. Starting with SWCNTs with polar rims, for the same inner diameter the tendency observed suggest that the larger nanotubes pierce spontaneously the bilayer faster if the hydrophobic mismatch with the bilayer is equal or below the bilayer hydrophobic thickness. For nanotubes showing a $\Delta_{HM}^{o} \geq 2.64\ nm$, the tendency is reversed, and the piercing time starts to increase with the length. An exception to this is observed for $\emptyset_{CNT} = 2.54\ nm$ when the length increases from $L_{CNT} = 5.39\ nm$ to $6.25\ nm$ ($L_{CNT}^{H} = 4.53\ nm$ and $5.39\ nm$, respectively). For the largest nanotube the piercing is faster again, even if the tilt is higher. The superior length seems to help on the internalization in the hydrophobic bilayer core producing a faster drag to the bottom monolayer. When comparing the inner diameters, when $\Delta_{HM}^{o} \leq 2.64\ nm$ the slowest piercing is observed for nanotubes with $\emptyset_{CNT} = 2.54\ nm$, while when $\Delta_{HM}^{o} \geq 2.64\ nm$ the slowest nanotubes to pierce are those with $\emptyset_{CNT} = 1.59\ nm$, coinciding with the highest tilt observed. As mentioned, the exception is observed for nanotubes of $L_{CNT} = 5.39\ nm$ and $\emptyset_{CNT} = 2.54\ nm$ exceeding $25\ ns$ for the complete

piercing. In the case of pristine SWCNTs, the piercing process is faster than for SWCNTs with polar rims. In all the simulations, the SWCNTs with polar rims pierce the first monolayer and start to tilt to maximize the contact between nanotube walls and lipid tails until the second monolayer is pierced too and the polar rims drive the stabilization by the interaction with the lipid head groups on the bottom monolayer. On the other hand, the visual sequence of the simulations shows that pristine SWCNTs pierce through the bilayer in a more perpendicular geometry, i.e. tilting less while being drag by the hydrophobic bilayer core.

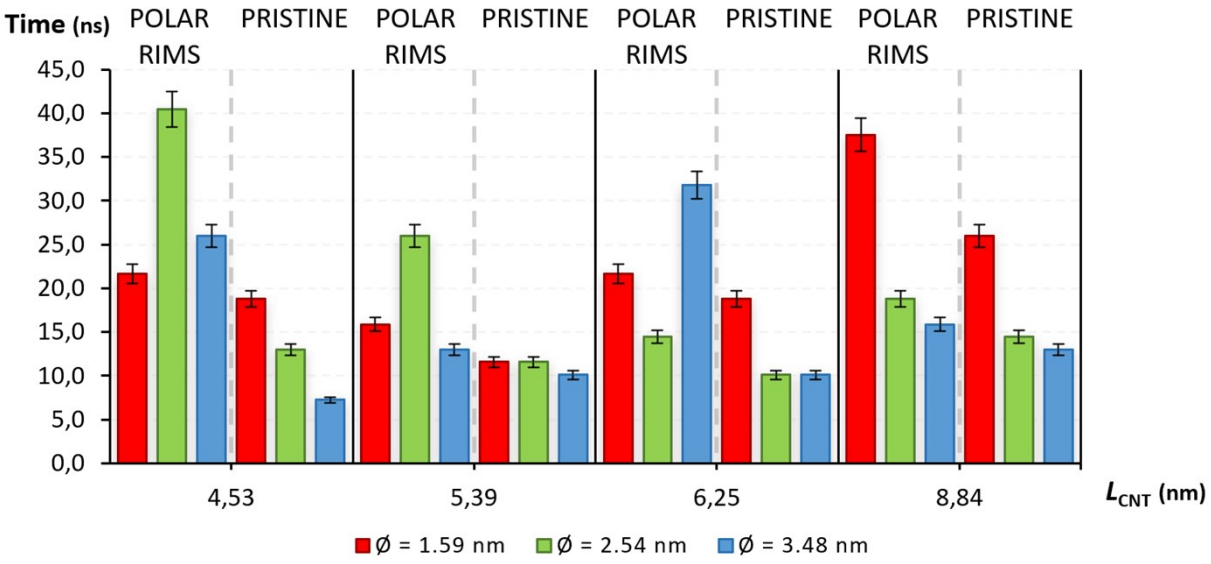

Fig. 3 SWCNT piercing time as function of nanotube total length L_{CNT} and diameter $Ø_{CNT}$ for both pristine SWCNTs (P.) and SWCNTs with polar rims (P.R.).

This "straight sinking" reduces the average piercing time, being the nanotubes of $Ø_{CNT} = 1.59\ nm$ the slowest among all the pristine SWCNTs simulated. For this diameter, as the nanotube length increase the piercing process becomes faster if $\Delta^{o}_{HM} \geq 3.53\ nm$, but only about $5\ ns$ faster. For larger nanotubes, the tendency is again reversed, and the piercing process becomes slower as the nanotube length increases. For the shorter nanotubes, as the inner diameter is increased the piercing becomes about $5\ ns$ faster for each higher diameter. When the length is increased, the diameter seems to lose importance and the process is slowed only for $Ø_{CNT} = 1.59\ nm$ as length increase. The piercing times for $Ø_{CNT} = 2.54\ nm$ and $3.48\ nm$ are highly similar for nanotube lengths above $L_{CNT} = L^{H}_{CNT} = 4.53\ nm$ with a maximum difference of $1.5\ ns$. The values for the obtained SWCNT angles θ_{CNT}, tilt angles θ_{tilt}, bilayer hydrophobic thickness d^{o}_{L}, and hydrophobic mismatch Δ^{o}_{HM} as well the plots of the calculated SWCNT angle θ_{CNT} as function of simulation time, can be found in this document in **Tables 6** and **7** as well in **Fig. 4** and **5**.

Due to the soft nature of the simulated particles, the nanotubes end filled with lipids and fully obstructed in some cases. Additional simulations have been done with all the SWCNTs considered initially placed perpendicular to the bilayer normal in a hole in the bilayer of size equal to each nanotube diameter, done by removing lipids from the bilayer. The results on

the tilt angles and stabilization are highly similar proving that the followed methodology is suitable for simulating functional SWCNT transmembrane channels through DPD.

Table 6 Calculated values of nanotube mean angle with respect the bilayer plane, mean tilt angle with respect to the bilayer normal from the stabilization point, pure bilayer hydrophobic thickness and hydrophobic mismatch for the simulated SWCNTs with polar rims piercing through a pure DMPC bilayer.

POLAR RIMS $d_{CNT}\,x\,\emptyset_{CNT}\,(nm)$	**Piercing** (ns)	θ_{CNT}	θ_{tilt} **(stabilized)**	**Stabilization** (ns)	$d_L^o(nm)$	$\Delta_{HM}^{o}\,(nm)$
4.53 x 1.59	21.7	82°	5°	293.1	2.684	0.979
5.39 x 1.59	15.9	84°	6°	37.5	2.701	1.824
6.25 x 1.59	21.7	61°	29°	44.8	2.698	2.689
8.84 x 1.59	37.5	34°	57°	98.2	2.775	5.198
4.53 x 2.54	40.4	84°	5°	115.5	2.702	0.961
5.39 x 2.54	26.0	83°	4°	209.3	2.724	1.801
6.25 x 2.54	14.4	71°	19°	52.0	2.725	2.662
8.84 x 2.54	18.8	39°	51°	75.1	2.784	5.189
4.53 x 3.48	26.0	86°	4°	233.9	2.720	0.943
5.39 x 3.48	13.0	86°	4°	98.2	2.744	1.781
6.25 x 3.48	31.8	77°	14°	65.0	2.752	2.635
8.84 x 3.48	15.9	44°	47°	89.5	2.803	5.170

Table 7 Calculated values of nanotube mean angle with respect the bilayer plane, mean tilt angle with respect to the bilayer normal from the stabilization point, pure bilayer hydrophobic thickness and hydrophobic mismatch for the simulated pristine SWCNTs piercing through a pure DMPC bilayer.

PRISTINE $d_{CNT}\,x\,\emptyset_{CNT}\,(nm)$	**Piercing** (ns)	θ_{CNT}	θ_{tilt} **(stabilized)**	**Stabilization** (ns)	$d_L^o(nm)$	$\Delta_{HM}^{o}\,(nm)$
4.53 x 1.59	18.8	74°	16°	34.6	2.704	0.959
5.39 x 1.59	11.5	42°	49°	82.3	2.706	1.819
6.25 x 1.59	18.8	33°	58°	50.5	2.720	2.667
8.84 x 1.59	26.0	10°	83°	128.5	2.780	5.193
4.53 x 2.54	13.0	79°	11°	46.2	2.733	0.930
5.39 x 2.54	11.5	53°	37°	34.6	2.734	1.791
6.25 x 2.54	10.1	40°	50°	40.4	2.749	2.638

8.84 *x* 2.54	14.4	18°	73°	187.7	2.816	5.157
4.53 *x* 3.48	7.2	81°	9°	46.2	2.761	0.902
5.39 *x* 3.48	10.1	62°	28°	39.0	2.769	1.756
6.25 *x* 3.48	10.1	45°	45°	50.0	2.787	2.600
8.84 *x* 3.48	13.0	31°	57°	495.2	2.869	5.104

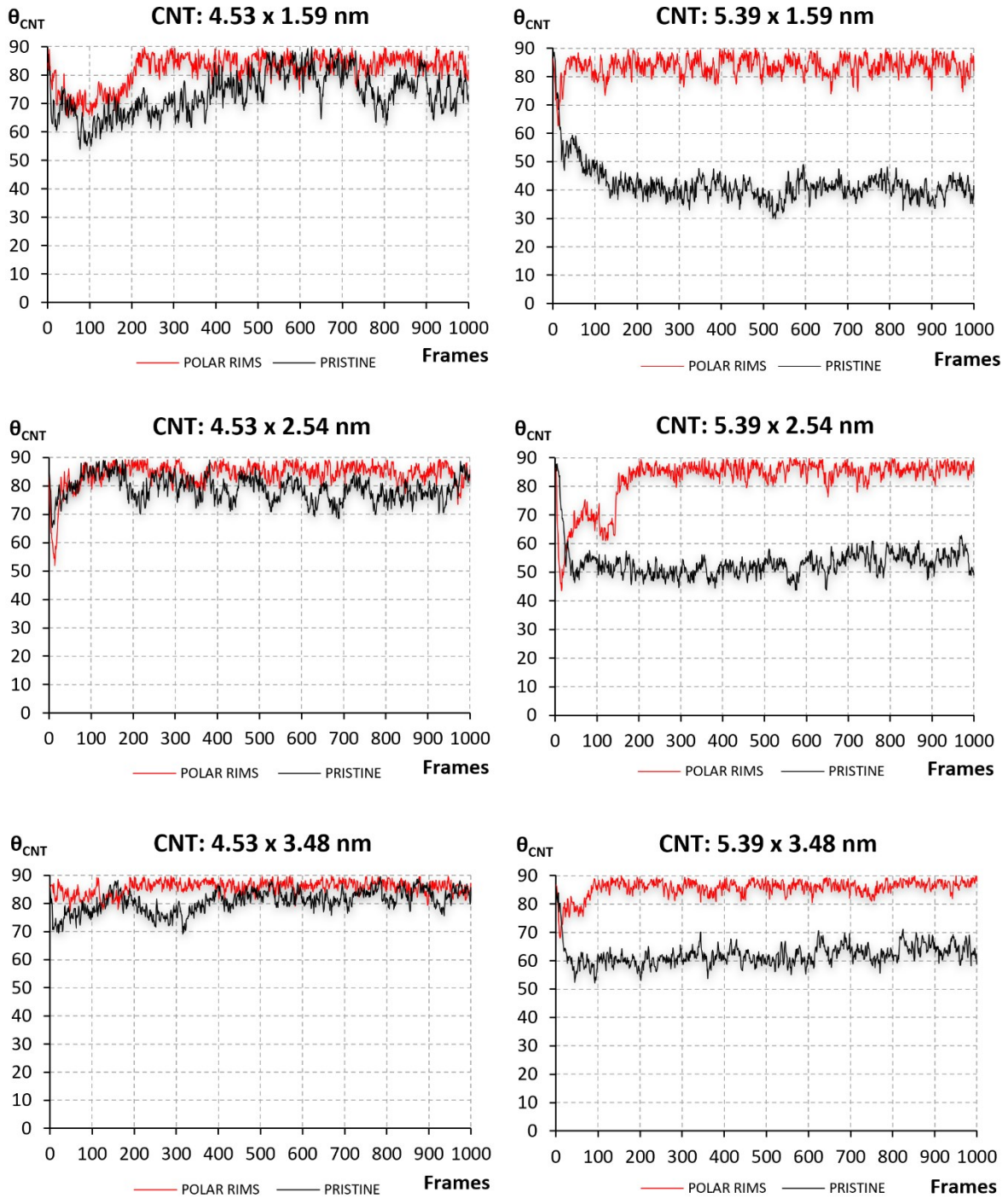

Fig. 4 Nanotube angle with respect the bilayer plane (yz) as function of simulation time in frames for SWCNTs of $4.53\ nm$ and $5.39\ nm$ length. Each frame corresponds to 300 DPD steps (10 cycles). The nanotube inner diameter as well its nature are indicated in each case.

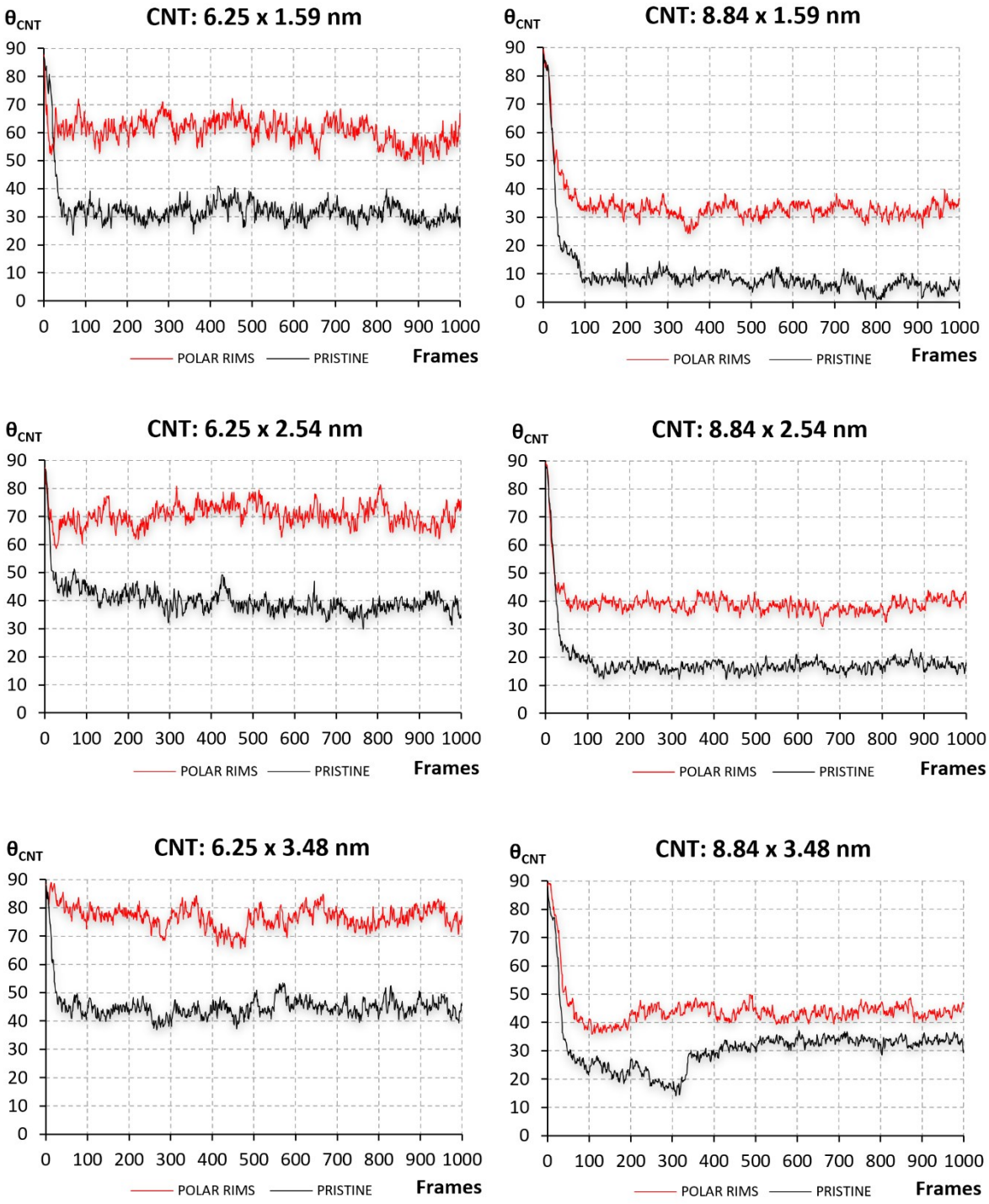

Fig. 5 Nanotube angle with respect the bilayer plane (yz) as function of simulation time in frames for SWCNTs of $6.25\ nm$ and $8.84\ nm$ length. Each frame corresponds to 300 DPD steps (10 cycles). The nanotube inner diameter as well its nature are indicated in each case.

ssDNA spontaneous internalization into SWCNT transmembrane channels

All the systems were simulated for 15000 cycles through conventional DPD, i.e. in the (N, V, T) ensemble, with a time step of $\delta t = 0.03\tau$ and a fixed number of 25 DPD steps per cycle. The ssDNA chains are placed initially centred and above the upper rim of each SWCNT in order to avoid the large simulation time that could take for the ssDNA to approach enough to the SWCNT to interact with. Moreover, a SWCNT with polar rims of $L_{CNT} = 5.39\ nm$ was used in all the simulations with the three inner diameters considered in this article. The temperature chosen for all the simulations with ssDNA was $T^* = 0.505$, i.e. $31.2\ °C$, the same than for SWCNT transmembrane channel simulations, since the aim in this section is to test the capability of the system for reproduce the translocation of other components through the pore by using DPD simulations. From visual inspection of the simulation using the software VMD,[20] the time needed for the total internalization of ssDNA chains into the SWCNTs as function of the inner diameter is determined. The point where all the beads composing the ssDNA are completely inside the SWCNT cavity and do not exit again, is used to confirm the internalization.

First, the random ssDNA sequences are examined and compare as function of their nucleic acid base content and the nanotube inner diameter. As shown in **Fig. 6**, the time needed for all chains to spontaneously enter completely in the nanotubes of $Ø_{CNT} = 1.59\ nm$, is far higher compared to the larger inner diameters as expected.

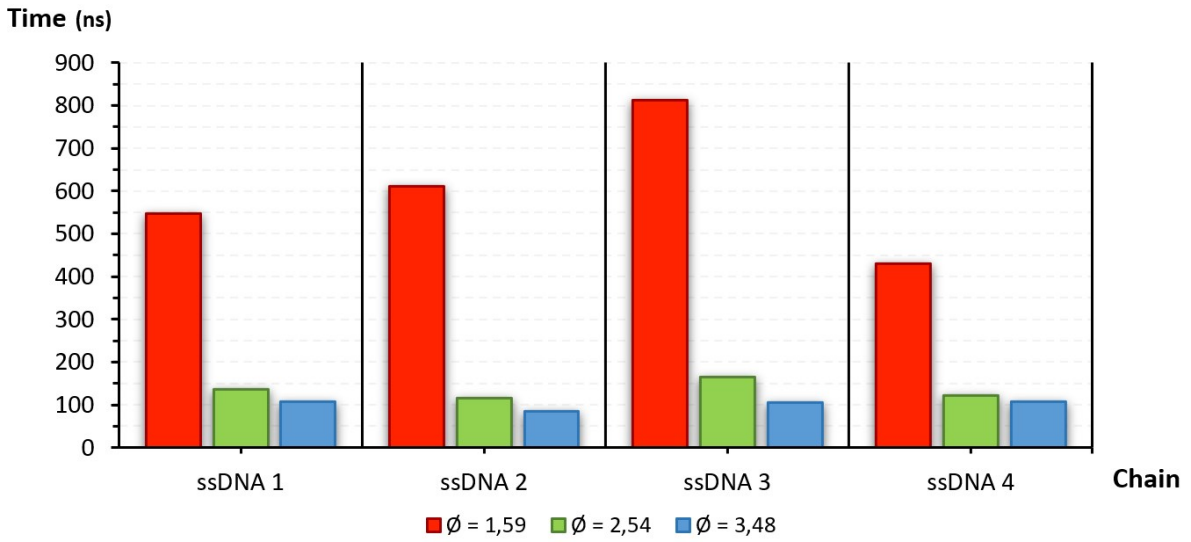

Fig. 6 Internalization time as function of the ssDNA chain sequence and the nanotube inner diameter. The nucleic acid content is indicated in **Table 2** in the published text.

From the DFT calculations, adenine and thymine are the nucleic acid bases with the highest hydration energies and therefore, the more hydrophobic nucleic acid bases. One could think that this fact would enhance its tendency to enter in the hydrophobic nanotube cavity but, while the ssDNA chain enters in the pore, water is also passing through it. Due to the limited free space into the nanotube once the chain starts to enter, the presence of water that are also crossing through the pore slows the ssDNA internalization by hydrophobic interactions with the nucleic acid bases, especially with adenine and thymine. Despite this, the ssDNA 4 chain with 32 % of adenine and 24 % of thymine is the faster entering into the nanotube needing about $430\ ns$, suggesting that the content in adenine and thymine is not the only factor to consider and the stochastic nature of DPD

technique may play a role in the behaviour of the system. The simulations for the ssDNA chains formed by a single nucleic acid base, as the time of internalization, are gathered in **Fig. 7**, which contain the average of three simulation for each chain.

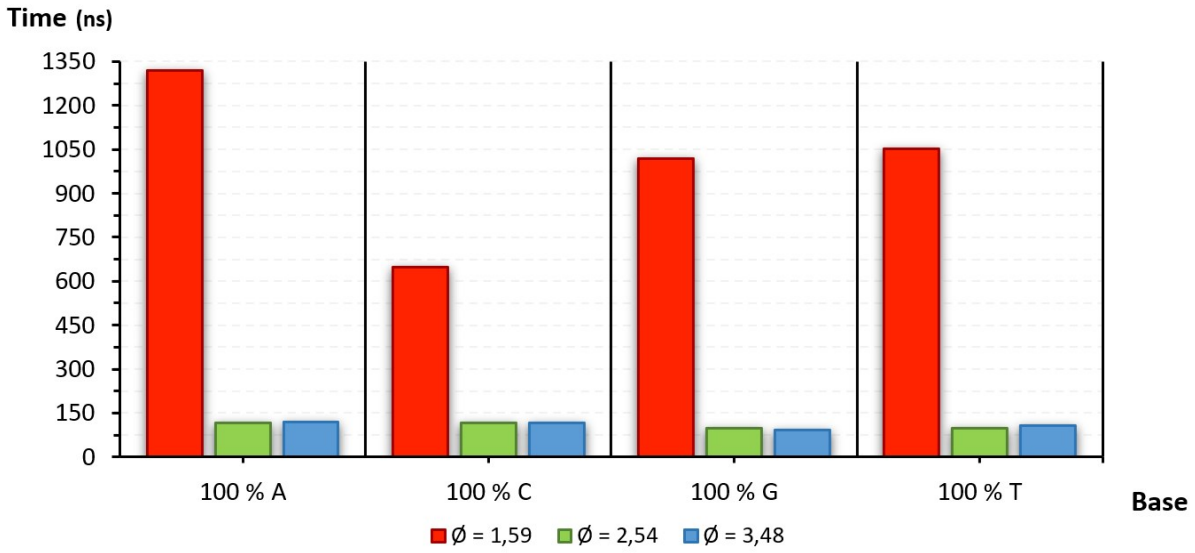

Fig. 7. Internalization time as function of the nucleic acid base content and the SWCNT inner diameter.

Snapshots of all the chains trapped in the corresponding SWCNTs from all the simulations, are shown in **Fig. 8-10** below. In **Fig 11**, the internalization process is shown as a sequence of snapshots for SWCNTs of $\emptyset_{CNT} = 2.54\ nm$ and $\emptyset_{CNT} = 3.48\ nm$ (the corresponding snapshots for $\emptyset_{CNT} = 1.59\ nm$ can be found in the main publication).

Fig. 8 Snapshots of all the simulated ssDNA chains inside SWCNTs of $\emptyset_{CNT} = 1.59\ nm$. The nanotubes are represented in lines in order to better visualize the ssDNA chain inside. For sake of clarity, the DMPC bilayer as well the water beads are not shown. The code of colours is: SWCNT polar rims, red lines; nanotube walls, grey lines; adenine, blue; cytosine, red; guanine, yellow; thymine, lime; phosphates, dark grey; pentoses, orange.

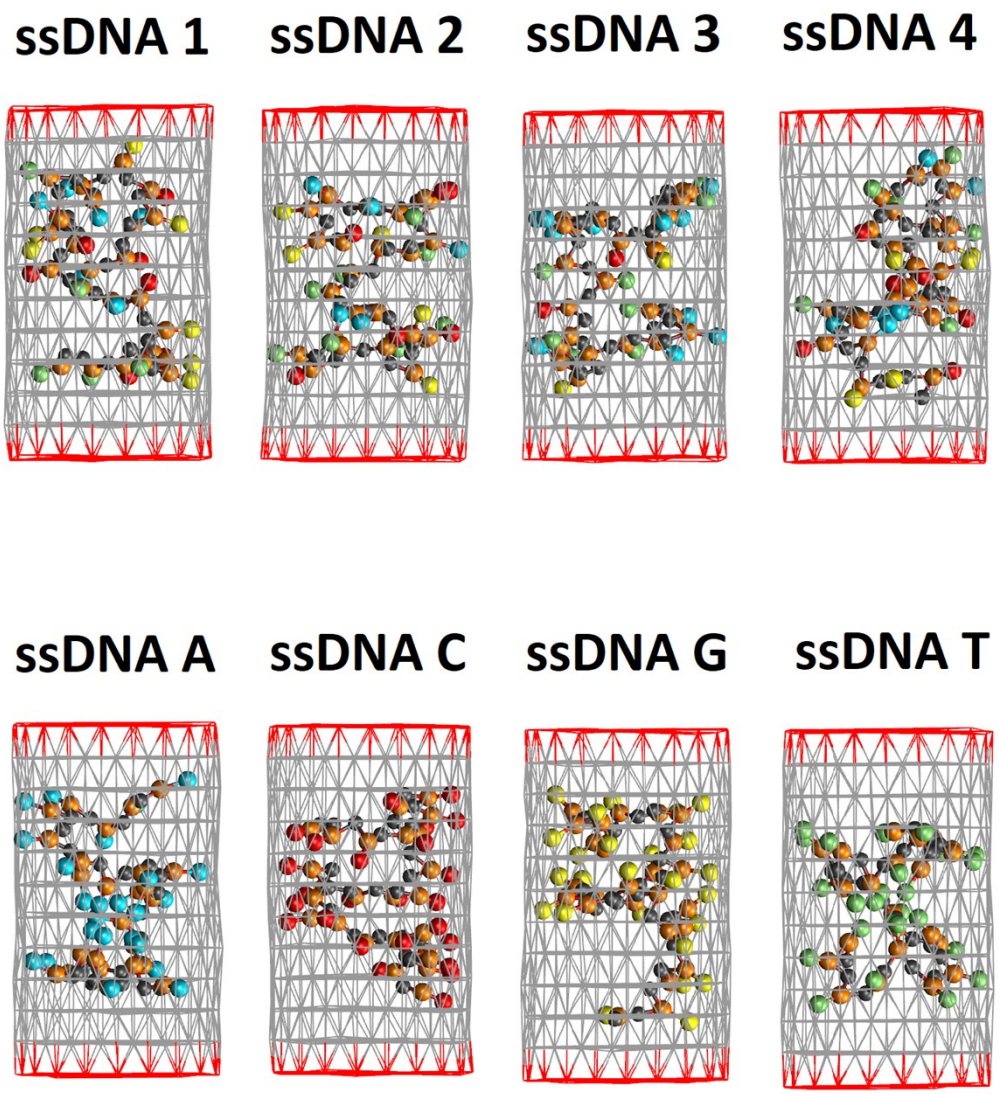

Fig. 9 Snapshots of all the simulated ssDNA chains inside SWCNTs of $\emptyset_{CNT} = 2.54\ nm$. The nanotubes are represented in lines in order to better visualize the ssDNA chain inside. For sake of clarity, the DMPC bilayer as well the water beads are not shown. The code of colours is: SWCNT polar rims, red lines; nanotube walls, grey lines; adenine, blue; cytosine, red; guanine, yellow; thymine, lime; phosphates, dark grey; pentoses, orange.

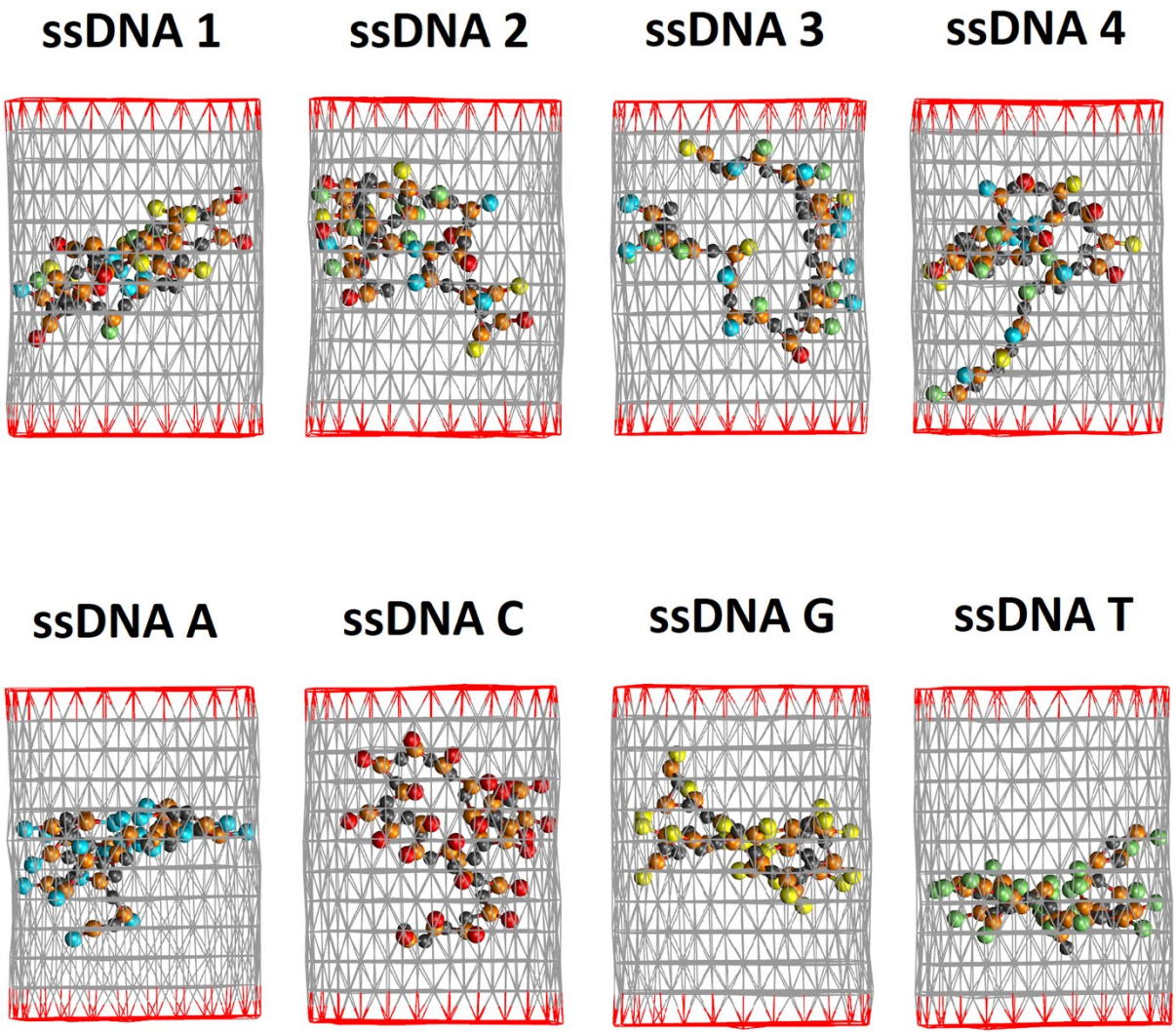

Fig. 10 Snapshots of all the simulated ssDNA chains inside SWCNTs of $\emptyset_{CNT} = 3.48\ nm$. The nanotubes are represented in lines in order to better visualize the ssDNA chain inside. For sake of clarity, the DMPC bilayer as well the water beads are not shown. The code of colours is: SWCNT polar rims, red lines; nanotube walls, grey lines; adenine, blue; cytosine, red; guanine, yellow; thymine, lime; phosphates, dark grey; pentoses, orange.

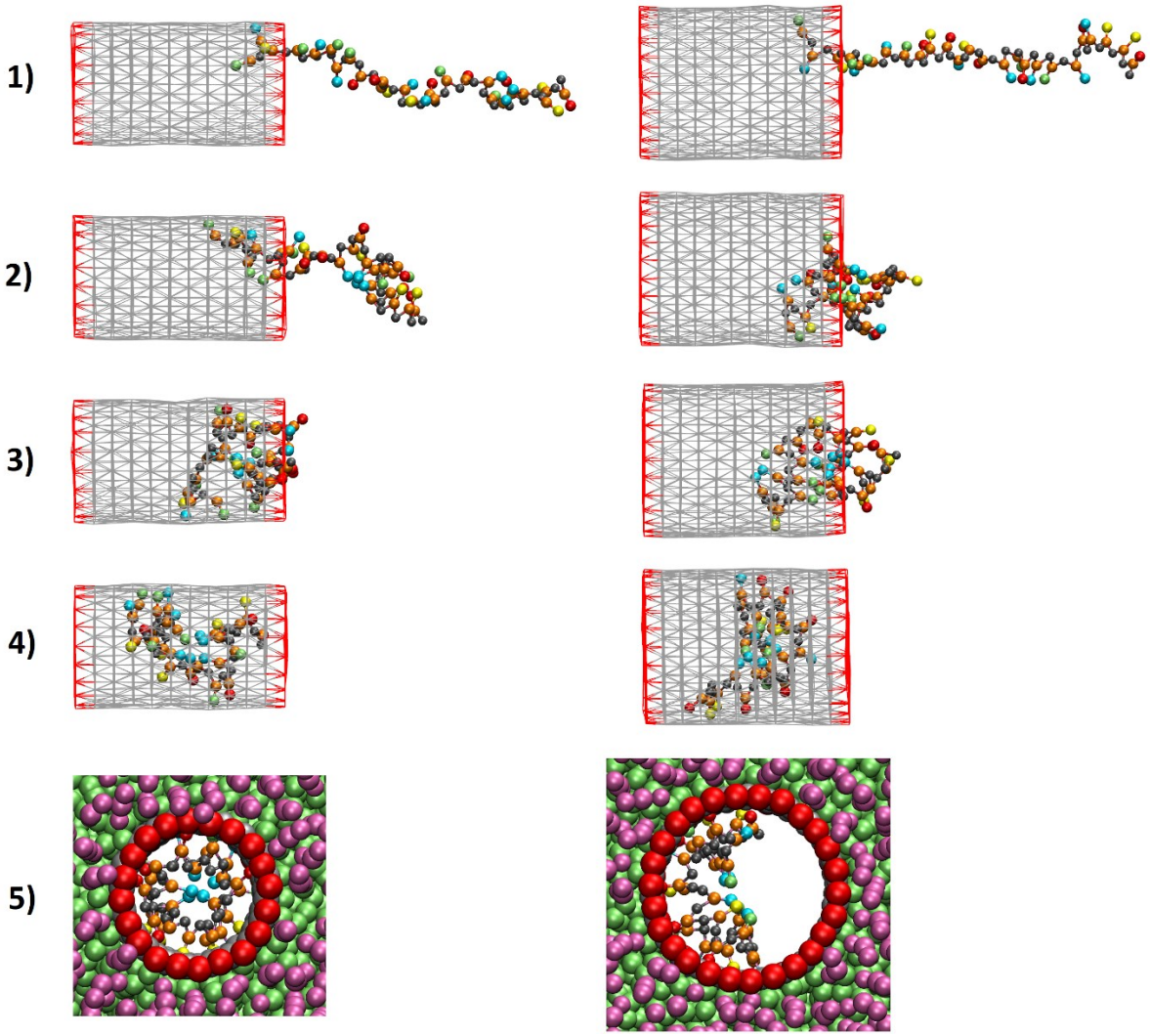

Fig. 11 Snapshots of the internalization process of one ssDNA into a SWCNT of $\emptyset_{CNT} = 2.54\ nm$ (left) and $\emptyset_{CNT} = 3.48\ nm$ (right). 1) first contact between one nucleic acid base and the nanotube inner walls; 2) internalization of the first part of the chain; 3) slow attachment of nucleic acid bases in the nanotube walls as the chain enters slowly; 4) ssDNA chain totally inside the nanotube and hydrophobically trapped in the inner hydrophobic pore; 5) upper view showing the SWCNT pierced in the bilayer and the ssDNA chain inside with the polar backbone centred in the pore and the nucleic acid bases interacting with the inner nanotube walls. For sake of clarity, the DMPC bilayer as well the water beads are not shown. The code of colours is: lipid head groups, mauve; lipid tails, lime; SWCNT polar rims, red lines; nanotube walls, grey lines; adenine, blue; cytosine, red; guanine, yellow; thymine, lime; phosphates, dark grey; pentoses, orange.

References

1 M. Kranenburg, M. Venturoli and B. Smit, *Physical Review E - Statistical Physics, Plasmas, Fluids, and Related Interdisciplinary Topics*, 2003, **67**, 3.

2 M. Kranenburg, J. P. Nicolas and B. Smit, *Physical Chemistry Chemical Physics*, 2004, **6**, 4142–4151.

3 M. Venturoli and B. Smit, *PhysChemComm*, 1999, **2**, 45–49.

4 F. de Meyer, J. Rodgers and T. Willems, *Biophysical journal*.

5 F. J. M. de Meyer, A. Benjamini, J. M. Rodgers, Y. Misteli and B. Smit, *Journal of Physical Chemistry B*, 2010, **114**, 10451–10461.

6 J. M. Rodgers, J. Sørensen, F. J. M. de Meyer, B. Schiøtt and B. Smit, *Journal of Physical Chemistry B*, 2012, **116**, 1551–1569.

7 A. Benjamini and B. Smit, *Soft Matter*, 2013, **9**, 2673–2683.

8 M. P. Allen and D. J. Tildesley, *Computer Simulation of Liquids*, Clarendon Press, 1987.

9 R. Groot and P. Warren, *The Journal of Chemical Physics*, 1997, **107**, 4423.

10 J. R. Lu, Z. X. Li, R. K. Thomas, E. J. Staples, I. Tucker and J. Penfold, *The Journal of Physical Chemistry*, 1993, **97**, 8012–8020.

11 R. D. Groot and K. L. Rabone, *Biophysical Journal*, 2001, **81**, 725–736.

12 J. R. PARTINGTON, R. F. HUDSON and K. W. BAGNALL, *Nature*, 1952, **169**, 583–584.

13 R. D. Groot, *Journal of Chemical Physics*, 2003, **118**, 11265–11277.

14 M. Venturoli, B. Smit and M. M. Sperotto, *Biophysical Journal*, 2005, **88**, 1778–1798.

15 R. Koynova and M. Caffrey, *Biochimica et Biophysica Acta - Reviews on Biomembranes*, 1998, **1376**, 91–145.

16 Tristram-Nagle, S.; Liu, Y.; Legleiter, J.; Nagle, J. F. *Biophys. J.* **2002**, *83* (6), 3324–3335.

17 Petrache, H. I.; Dodd, S. W.; Brown, M. F. *Biophys. J.* **2000**, *79* (6), 3172–3192.

18 Kučerka, N.; Nieh, M. P.; Katsaras, J. *Biochim. Biophys. Acta - Biomembr.* **2011**, *1808* (11), 2761–2771.

19 Nagle, J. F.; Tristram-Nagle, S. *Biochim. Biophys. Acta - Rev. Biomembr.* **2000**, *1469* (3), 159–195.

20 Attaf, B., *An Eco-Approach to Boost the Sustainability of Carbon Nanotube-Based Composite Products. world Acad. Publ. Co. Ltd.,* **2016**, 1-14.

21 T. A. Knotts, N. Rathore, D. C. Schwartz and J. J. de Pablo, *Journal of Chemical Physics,* **2007**, 126 (8), 84901.

22 S. Arnott, P.J. Campbell-Smith & R. Chandrasekaran. In Handbook of Biochemistry and Molecular Biology, 3rd ed. Nucleic Acids--Volume II, G.P. Fasman, Ed. Cleveland: CRC Press. **1976**. pp. 411-422.

23 A. M. Ababneh, C. C. Large and S. Georghiou, *Biophysical Journal*, 2003, **85**, 1111–1127.